npj | climate and atmospheric science

www.nature.com/npjclimatsci

ARTICLE OPEN

Check for updates

Seasonal to decadal variations of precipitation oxygen isotopes in northern China linked to the moisture source

Fangyuan Lin[1,2,3], Qiong Zhang[3]✉, Ashish Sinha[4], Zhenqian Wang[3], Josefine Axelsson[3], Lvfan Chen[1,2], Tianli Wang[1,2] and Liangcheng Tan[1,5]✉

A precise characterization of moisture source and transport dynamics over the inland margins of monsoonal China is crucial for understanding the climatic significance of precipitation oxygen isotope ($\delta^{18}O_p$) variability preserved in the regional proxy archives. Here, we use a general circulation model with an embedded water-tagging module to quantify the role of moisture dynamics on the seasonal to decadal variations of $\delta^{18}O_p$ in northern China. Our data indicate that during the non-monsoon season, the $\delta^{18}O_p$ variability is dominated by the temperature effect. Conversely, in the summer monsoon season, the moisture contributions from the low-latitude land areas (LLA), the Pacific Ocean (PO), and the North Indian Ocean (NIO) override the temperature effect and influence the summer $\delta^{18}O_p$. Intensified upstream convection along the NIO moisture transport pathway results in a more negative summer $\delta^{18}O_p$ compared to moisture transported from the PO and LLA regions. Our analysis shows a decadal shift in summer $\delta^{18}O_p$ around the mid-1980s, marking changes in the relative contribution of oceanic moisture from PO and NIO in response to changes in the atmospheric circulation patterns influenced by the Pacific Decadal Oscillation. We suggest that such decadal-scale $\delta^{18}O_p$ variability can be recorded in the natural archives from the region, which can provide valuable insights into understanding past climate variability.

npj Climate and Atmospheric Science (2024)7:14 ; https://doi.org/10.1038/s41612-024-00564-x

INTRODUCTION

The oxygen isotopic composition of precipitation ($\delta^{18}O_p$) recorded in natural archives, such as ice cores, speleothems, and tree rings, is one of the most widely used proxies for reconstructing past climate change. Despite its widespread application, the climatic significance of $\delta^{18}O_p$ and stalagmite $\delta^{18}O$ ($\delta^{18}O_s$) records, especially in the context of the East Asian summer monsoon (EASM), has been the subject of much debate[1–5]. The orbital to millennial variations of $\delta^{18}O_p$ and $\delta^{18}O_s$ in the EASM region are thought to be primarily influenced by the large-scale circulation and latitudinal migration of the EASM rain belt, ultimately showing integrated monsoonal signals from the moisture source to the cave sites[1,4,6,7]. Nevertheless, a consensus understanding of various hydrological processes governing variations in EASM $\delta^{18}O_p$ and $\delta^{18}O_s$ on short timescales has not been reached. Studies employing modern observations and general circulation model water isotope modeling have attributed seasonal to decadal $\delta^{18}O_p$ and $\delta^{18}O_s$ variability to multiple factors, including "upstream" processes[8–11], moisture source dynamics[12,13], local precipitation amount[14], and precipitation seasonality[15–17]. These diverse interpretations highlight the complexities inherent in $\delta^{18}O_p$ and $\delta^{18}O_s$, which may differ across monsoonal China, especially between the northern and southern regions.

Northern China, located at the margin of the EASM region, experiences a more continental climate. In contrast to typical EASM areas, the $\delta^{18}O_p$ in this region displays a different seasonal variation, exhibiting a pattern of depleted values in winter and relatively enriched values in summer[18]. However, the understanding of the seasonal $\delta^{18}O_p$ patterns in northern China remains incomplete due to a scarcity of modern observational records. Initially, the seasonal $\delta^{18}O_p$ variability in northern China was explained in terms of local climate conditions following the paradigm of the "temperature effect" and "amount effect"[19,20]. Furthermore, recycled moisture from local evapotranspiration was also considered as a contributing factor[21–23]. However, the relationships between $\delta^{18}O_p$ and local conditions may be masked by the complex, large-scale processes, such as moisture sources and upstream convection. Li et al.[24] proposed that the "temperature effect" exists during the non-monsoon season, while summer $\delta^{18}O_p$ can be affected by upstream convection. Tang et al.[25] suggested that the interplay of moisture source and upstream rainout contribute to the variation of summer $\delta^{18}O_p$. While Zhang et al.[18] and Wang et al.[26] suggested a minimal influence of upstream convection on the $\delta^{18}O_p$ in northern China. They proposed that the seasonal $\delta^{18}O_p$ cycle in northern China is driven by a shift in westerly-derived continental moisture to the Pacific Ocean moisture, with the single continental air mass during the non-monsoon season being more susceptible to the temperature effect[18,26]. Moreover, Xie et al.[27] suggested that the summer $\delta^{18}O_p$ is not affected solely by Pacific moisture but rather the remote monsoonal sources like the Indian Ocean and the Bay of Bengal moisture. Contrarily, westerly-derived continental moisture can prevail throughout the year during weak monsoon periods, underscoring the intricate moisture dynamics at the margin of the EASM area[28]. Overall, the influence of moisture source dynamics on $\delta^{18}O_p$ varies spatially[12]. It remains uncertain whether and how the varying moisture sources have a discernible effect on the $\delta^{18}O_p$ in northern China.

Here, we use the Community Atmosphere Model version 3 (CAM3), with embedded water-tagging and stable water isotopes

[1]State Key Laboratory of Loess and Quaternary Geology, Institute of Earth Environment, Chinese Academy of Sciences, Xi'an 710061, China. [2]University of Chinese Academy of Sciences, Beijing 100049, China. [3]Department of Physical Geography and Bolin Centre for Climate Research, Stockholm University, Stockholm 10691, Sweden. [4]Department of Earth Sciences, California State University, Dominguez Hills, Carson 90747 CA, USA. [5]Institute of Global Environmental Change, Xi'an Jiaotong University, Xi'an 710049, China. ✉email: qiong.zhang@natgeo.su.se; tanlch@ieecas.cn

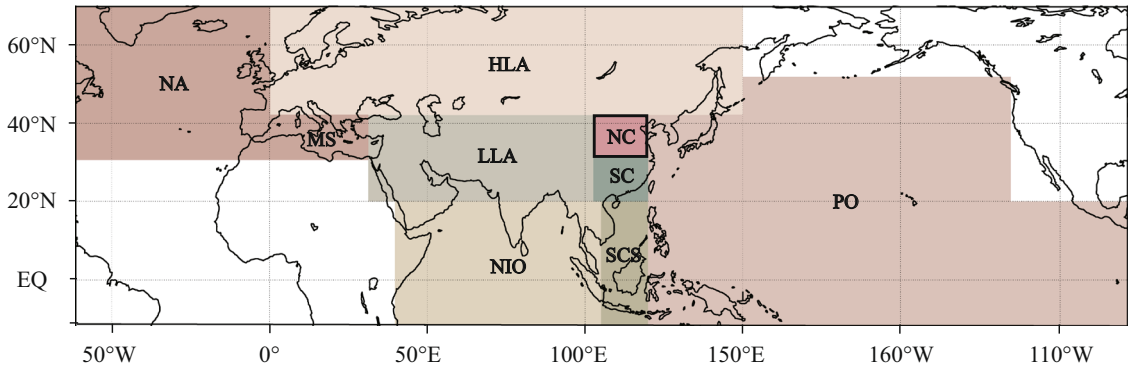

Fig. 1 Schematic representation of moisture source regions considered in this study. The eight moisture sources including high-latitude land area (0–150°E, 42–70°N, HLA), northern China (102–120°E, 32–42°N, NC), southern China (102–120°E, 20–32°N, SC), low-latitude land area (30–105°E, 20–42°N, LLA), Mediterranean Sea & North Atlantic Ocean (0–30°E, 30–42°N & 60°W–0°, 30–70°N, M_N), Pacific Ocean (120°E–125°W, 20–50°N, 120°E–90°W, 10°S–20°N, PO), South China Sea (105–120°E, 10°S–20°N, SCS), North Indian Ocean (40–105°E, 10°S-20°N, NIO). The black box represents the defined areas for northern China.

modules, to trace the journey of water vapor from the evaporation in the source region to precipitation in the target region without the time limitation for tracing water vapor parcels[29] (see Methods for details). Our primary objectives encompass identifying the sources of water vapor in northern China, quantitatively analyzing moisture source variability, and evaluating their influence on the seasonality of $\delta^{18}O_p$. Additionally, we aim to establish connections between the moisture sources and the decadal variations observed in $\delta^{18}O_p$.

RESULTS

Experiments design

The CAM3 simulation has been effectively validated for various regions and is extended here to precipitation and $\delta^{18}O$ in precipitation and water vapor ($\delta^{18}O_v$) in northern China. Spanning 70 years (1951–2020), the simulation successfully reproduces climatology and annual cycle in precipitation and $\delta^{18}O$ over northern China with impressive accuracy, which is directly comparable to the observational data (see Supplementary discussion, Supplementary Figs. 1–5), indicating that CAM3 is highly effective in reproducing large-scale moisture dynamics and hydrological cycle over the northern China.

Based on previous studies[24,30], eight potential moisture sources are selected to account for the precipitation falling within northern China. These regions encompass high-latitude land areas (HLA), northern China (NC), southern China (SC), low-latitude land areas (LLA), Mediterranean Sea (MS) & North Atlantic Ocean (NA), Pacific Ocean (PO), South China Sea (SCS), and North Indian Ocean (NIO) (Fig. 1). The contribution from the rest of the globe is calculated as the residual between the precipitation of the target region and the sum of the precipitation that originates from the eight moisture sources. We define the area from 32°N–42°N and 102°E–120°E as the target region.

Influence of local meteorological conditions on $\delta^{18}O_p$

In the context of the predominantly continental climate in northern China, the local meteorological factors may play a vital role in shaping the $\delta^{18}O_p$ seasonality[31]. Strong relationships between temperature and $\delta^{18}O_p$ have been confirmed in northern China from International Atomic Energy Agency data[32]. Such a relationship exists in our data for the non-monsoon seasons. A positive correlation between monthly weighted average $\delta^{18}O_p$ and temperature was observed in winter (NDJF), pre-monsoon (MAM), and post-monsoon (SO) periods in CAM3 simulation (Table 1). Notably, the temperature effect diminishes during the summer monsoon season (JJA), coinciding with a significant increase in precipitation. While previous studies have suggested that the amount effect overshadows the temperature effect during this period[20], our findings propose that the influence of precipitation amount on $\delta^{18}O_p$ appears relatively weak (Table 1). These results suggest that the local meteorological factors cannot fully explain the variations of the $\delta^{18}O_p$. It is imperative to consider other large-scale processes, including moisture sources, transport distances, and upstream convection.

Table 1. The Pearson correlation between the amount weighted $\delta^{18}O_p$ and local meteorological factors.

$\delta^{18}O_p$	NDJF	MAM	JJA	SO
Temperature	0.25*	0.30*	0.12	0.42*
Precipitation	0.13	0.28*	−0.19	−0.27*

Asterisks (*) means significant at 95% confidence level (one-tailed, *t* test; after accounting for autocorrelation).

Climatology of moisture contributions

In this section, we quantify the relative contributions of moisture from the eight source regions to northern China. The annual cycles of simulated moisture contributions to total precipitation (longitudinally averaged from 102°E to 120°E) from each tagged region between 10°N to 50°N are illustrated in Hovmöller diagrams (Fig. 2e). During the non-monsoon season, moisture contributions to northern China are primarily from PO (~22–34%) and LLA (~25–32%) source regions (i.e., recycled vapor originating from low latitude land surfaces (Fig. 2).

Previous studies have indicated that the westerlies serve as a primary carrier of water vapor transport in northern China during the non-monsoon season, with the Atlantic Ocean, Black Sea, Caspian Sea, and recycled moisture during the pathway being the main moisture sources[27,33]. Despite the strength of the westerlies, some studies have pointed out that the main source of winter precipitation is oceanic moisture from the eastern transport[12]. Our results suggest a combined continental and oceanic moisture contribution during the non-monsoon season, with the westerlies and western Pacific subtropical high (WPSH) playing key roles[26,34,35]. The westward flow of western Pacific moisture, driven by the WPSH (depicted by the blue dashed line in Fig. 3), intersects with LLA moisture driven by the southern branch of tropospheric westerlies, known as the India-Burma trough

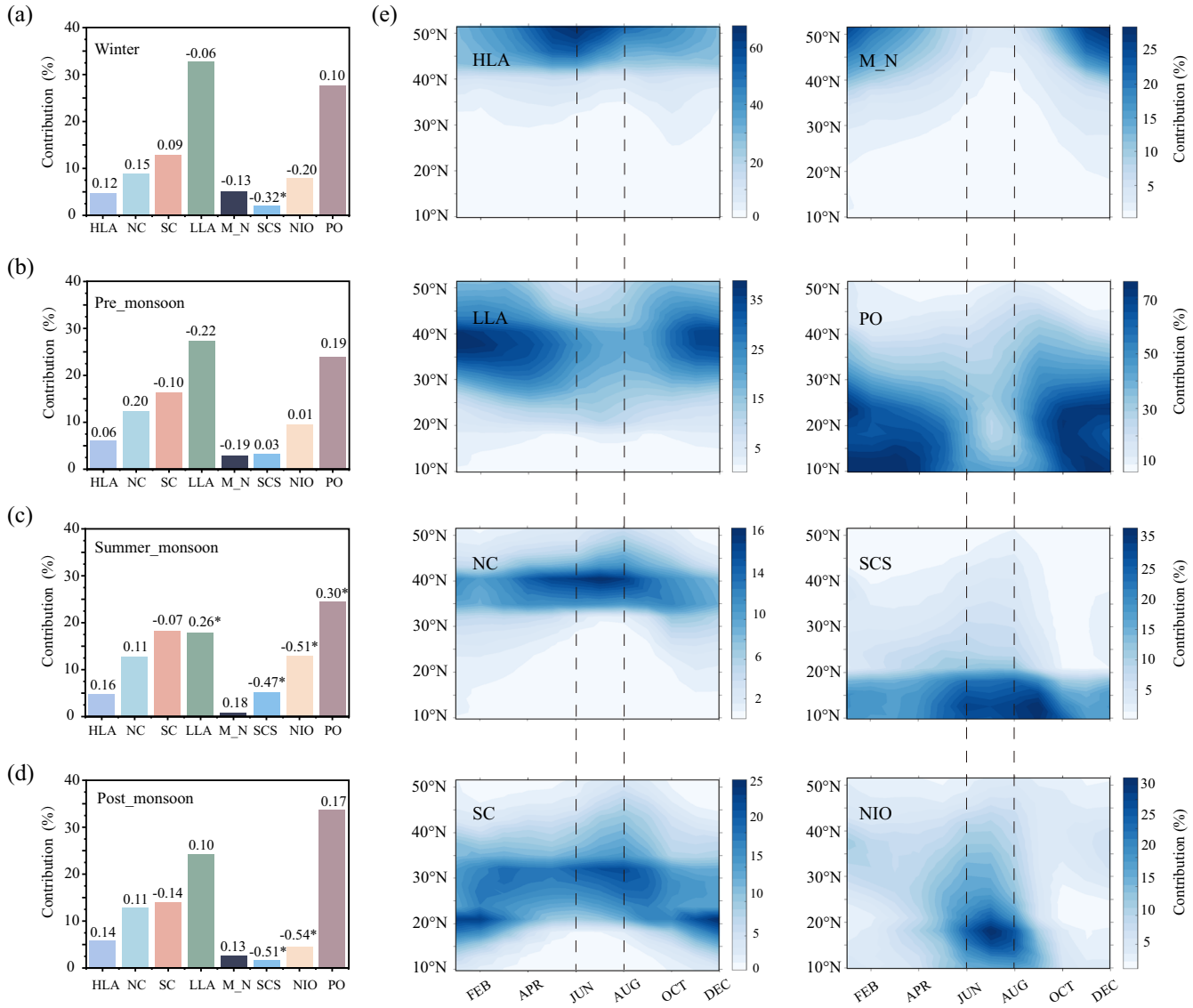

Fig. 2 Results from the CAM3 tagging simulation. Histograms showing relative contributions of each vapor source (%) to total precipitation averaged over northern China for winter (**a**), pre-monsoon (**b**), summer monsoon (**c**), and post-monsoon (**d**) seasons. The Pearson correlation between CAM3 simulated monthly anomalies of amount weight oxygen isotopic composition of precipitable ($\delta^{18}O_p$) and contribution (%) for each vapor source was marked, * means significant at 95% confidence level (one-tailed, *t* test; after accounting for autocorrelation). Moisture sources that contribute less than 10% are considered minimal effects. **e** Hovmöller diagram showing the seasonal evolution of tagged vapor contribution (%) from each source region (longitudinally averaged between 102°E and 120°E) and spanning between 10°N and 55°N. Dotted black lines highlight the June to August monsoon season. The period of the analysis is from 1951 to 2020.

(depicted by the red dashed line in Fig. 3), deflecting moisture northward to northern China.

During the summer monsoon season, the cross-equatorial low-level jet intensifies, serving as the dominant pathway of moisture transport across the equatorial Indian Ocean and the Arabian Sea into northern China (white dashed line, Fig. 3), and the moisture contribution from NIO significantly increases (~13%). In contrast, the moisture contribution from the LLA region decreases (~18%) due to the weakening of westerlies (Figs. 2 and 3). The contribution from the PO remains relatively consistent at around 24%, which is attributed to the development and reinforcement of the western and equatorial Pacific moisture channel with the formation of EASM[18,36]. This channel converges with the NIO channel at about 110°E and turns northward, transporting the PO moisture to northern China (blue dashed line, Fig. 3). Overall, the contribution of land moisture decreases significantly during summer monsoon season, the PO and the NIO become the major oceanic water vapor contributors.

Influence of moisture contribution and upstream convection on $\delta^{18}O_p$

Linear correlations between monthly weighted $\delta^{18}O_p$ and moisture contributions from each tagged source region are summarized in Fig. 2. During the non-monsoon season, the moisture source contributions exhibit a minor impact on the $\delta^{18}O_p$ values. With relatively stable moisture sources and low precipitation amount, the temperature-dependent isotope fractionation assumes significance, making temperature the

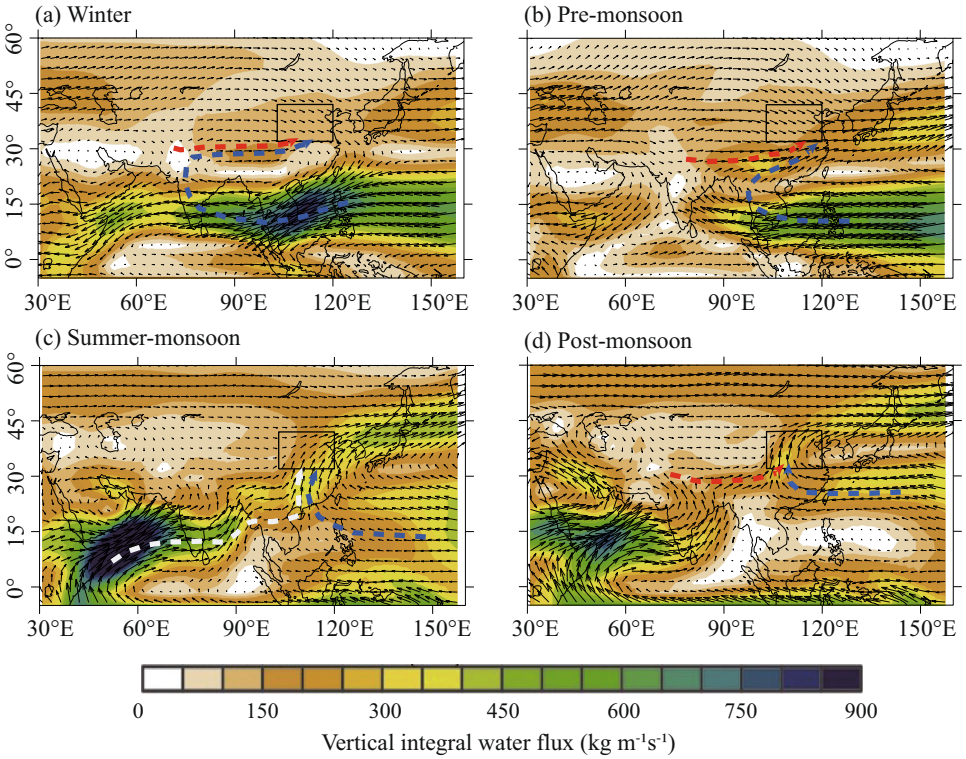

Fig. 3 Climatological water vapor flux patterns from CAM3 (1951–2020). Vertical integral water vapor flux (shaded and arrows) climatology for winter (**a**), pre-monsoon (**b**), summer monsoon (**c**), post-monsoon (**d**) from CAM3. The blue dashed line indicates the Pacific Ocean moisture channel, the red dashed line indicates the westerlies moisture channel, and the white dashed line indicates the North Indian Ocean moisture channel.

Table 2. The Pearson correlation between the amount weighted $\delta^{18}O_p$ and each initial moisture $\delta^{18}O_v$.

$\delta^{18}O_v$	HLA	NC	SC	LLA	MN	PO	SCS	NIO
MAM	0.16	0.69*	0.12	0.22	−0.24	−0.06	−0.21	−0.13
JJA	0.19	0.32*	0.00	0.22	−0.06	0.13	−0.04	0.06
SO	0.18	0.64*	0.23	0.29*	0.03	0.01	−0.03	0.12
NDJF	0.05	0.14	0.13	−0.12	0.04	00.00	−0.03	−0.07

Asterisks (*) means significant at 95% confidence level (one-tailed, *t* test; after accounting for autocorrelation).

primary factor driving $\delta^{18}O_p$ variations. However, during the summer monsoon season, the influence of moisture sources becomes apparent. Specifically, summer $\delta^{18}O_p$ exhibits a notable negative correlation with NIO moisture contribution ($r \sim -0.51$), and a positive correlation with contributions from PO and LLA source regions ($r \sim 0.30$ and 0.26, respectively) (Fig. 2c).

These correlations might be attributed to differences in the initial moisture $\delta^{18}O_v$ values in the source region[30]. Contrary to the expectation, our analysis reveals no significant correlation between the initial $\delta^{18}O_v$ of each moisture and $\delta^{18}O_p$ in northern China (Table 2). While there is a positive correlation between local $\delta^{18}O_v$ and $\delta^{18}O_p$, this is more likely due to local processes. Thus, we conclude that the initial moisture $\delta^{18}O_v$ signal does not exert a discernible influence on $\delta^{18}O_p$ in northern China. Instead, modification of the initial moisture $\delta^{18}O_v$ along the trajectories toward the sink region plays a pivotal role[37].

Transport distance from moisture sources to the sink region is proposed to influence EASM $\delta^{18}O_p$, with extended Indian Ocean moisture leading to depleted $\delta^{18}O_p$ value, while adjacent western Pacific Ocean moisture exhibits an opposing effect[13,38]. However, in the context of the vast area of defined PO moisture, the transport distance may act as a secondary contributing factor. More significantly, upstream convective rainout processes during the water vapor transport pathway, affected by the seasonal movement of the Intertropical Convergence Zone, have the potential to alter the precipitation and vapor isotope compositions in the upstream regions, subsequently extending this influence to downstream sites[8–10,37,39,40].

So far, it remains uncertain whether upstream convection affects $\delta^{18}O_p$ variation in northern China due to the extended distance from the tropical convection zone[18,26]. To address this, we analyzed the relationship between $\delta^{18}O_p$ and $\delta^{18}O_v$ in northern China and outgoing longwave radiation (OLR) as an indicator for convection intensity[41]. During the summer monsoon season, we find significant positive correlations between $\delta^{18}O_p$ and OLR in most of the NIO source region, suggesting that lower $\delta^{18}O_p$ is associated with stronger convection in this rainout zone (Fig. 4). These high correlation areas cover especially in the India sub-continent, Bay of Bengal and Arabian Sea (Fig. 4), where the convection is the most active[24,26,42]. When evaporated vapor moves through the convection zone, deep convection-induced intensified re-evaporation or enhanced downdrafts, carrying lighter vapor from upper atmospheric layers, could lead to a depletion of the NIO $\delta^{18}O_v$[10,43,44]. This influence is subsequently propagated to and impacts the $\delta^{18}O_p$ in downstream areas. Therefore, the isotopically depleted NIO moisture, caused by the intensified upstream convection process during the moisture transport

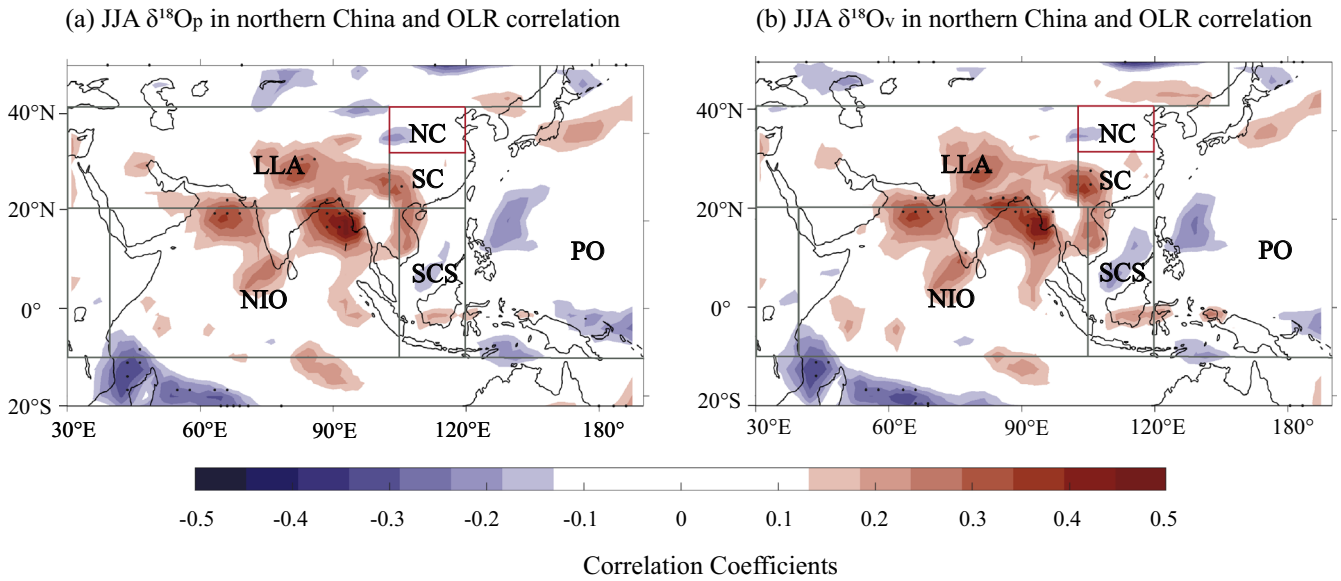

Fig. 4 Spatial correlation fields of CAM3 simulated $\delta^{18}O$ in northern China and outgoing longwave radiation. a Spatial correlations between CAM3 simulated JJA amount weighted precipitation $\delta^{18}O$ ($\delta^{18}O_p$) in northern China and JJA outgoing longwave radiation (OLR) at each grid cell. **b** Same as **a** but for CAM3 simulated water vapor $\delta^{18}O$ ($\delta^{18}O_v$) at lower-troposphere (1000–750 hPa) in JJA. The red rectangular is the defined sink region (102°–120°E, 32°–42°N). The correlation was performed after removing the climatological mean and trend from the data. Stippling represents data points that are statistically significant at the 95% confidence level obtained after accounting for serial correlations in data at each grid point followed by the application of FDR procedure with a 5% threshold (see "Methods"). FDR represents the anticipated fraction of null hypotheses that are mistakenly rejected in multiple-hypothesis testing.

pathway, contributes to negative summer $\delta^{18}O_p$ values in northern China in comparison with moisture transported from PO and LLA, which typically feature enriched $\delta^{18}O_v$.

Moisture control on decadal variability of summer $\delta^{18}O_p$

The $\delta^{18}O_p$ in East Asia has been proposed as a reliable index of EASM activity[2–5,13], considering the minimal contribution of non-monsoon precipitation in the northern region[17], we use the summer $\delta^{18}O_p$ ($\delta^{18}O_{p\_JJA}$) as an index of EASM intensity. The northern China $\delta^{18}O_{p\_JJA}$ exhibits a decadal-scale weakening in the EASM intensity during the mid-1980s (Fig. 5a), which is observed across EASM region (Supplementary Fig. 6). Changes in the amplitude of decadal EASM variability over the twentieth century have been associated with significant changes in precipitation pattern over eastern China[45–47]. Previous studies have shown that the decadal-scale climate variability over the twentieth century was partly attributable to changes in regional water vapor transport[30,47,48]. The Pacific Decadal Oscillation (PDO)[49–51], and the SST warming over the North Atlantic Ocean[52] are considered the main influencing factors. The correlation between 7-year low-filtered $\delta^{18}O_{p\_JJA}$ and global SST indeed resembles a PDO pattern (Supplementary Fig. 7). Therefore, we focus on the PDO phase transition on the $\delta^{18}O_{p\_JJA}$ pattern and moisture supply in northern China.

We use composite analysis to examine decadal variations in $\delta^{18}O_{p\_JJA}$ and the related moisture contributions from each tagged source over northern China during different PDO phases. Two periods before and after 1985 (i.e., 1967–1984 and 1985–2002) are selected as the typical cold and warm PDO phases. Figure 5 shows the synergistic decadal variation between the $\delta^{18}O_{p\_JJA}$ and summer precipitation ($r \sim -0.48$, 7-year low-filtered). The warm PDO phase is characterized by positive $\delta^{18}O_{p\_JJA}$ values and reduced precipitation amount in northern China, and vice versa for the cold PDO phase (Fig. 5a, b). During the warm PDO phase, PO moisture converges over most of the EASM domain due to a weaker and/or eastward-shifted WPSH[53] (Fig. 6b). On the other hand, moisture contribution from NIO is substantially reduced over northern China as a result of weakened low-level circulation (Fig. 6a). There is also a reduction of land recycled moisture, especially the local recycled moisture (Fig. 6c). In contrast, moisture from LLA, HLA, M_N, SC, and SCS shows a minor variation (Supplementary Figs. 8 and 9). These alternations are more significant in the moisture contribution compared to the change in water vapor volume (Fig. 6d–f).

We also examine how variations in moisture contributions from NIO, PO, and NC (local recycled moisture) affect the decadal variation of $\delta^{18}O_{p\_JJA}$, as these three moisture sources show the largest change between warm and cold PDO phases. During warm PDO phases, diminished isotopically depleted NIO moisture coupled with the increased isotopically enriched PO moisture result in enriched $\delta^{18}O_{p\_JJA}$ over northern China (Figs. 5 and 6). Notably, local recycled moisture is substantially reduced during the warm PDO phase (Fig. 6c, f). However, the lack of correlation with $\delta^{18}O_{p\_JJA}$ (Fig. 2c) implies that the reduction doesn't necessarily result in enriched $\delta^{18}O_{p\_JJA}$, which could be attributed to the possibility that local recycled moisture comes from transpiration instead of evaporation[54]. Therefore, the local recycled moisture does not significantly influence the decadal variation of $\delta^{18}O_{p\_JJA}$. However, reduced local recycled and NIO moisture, despite increased PO moisture, contributes to decreased precipitation in northern China (Figs. 5 and 6). Both large-scale atmospheric circulation and local processes thus govern the decadal variation of precipitation in northern China. Different from precipitation, the decadal $\delta^{18}O_{p\_JJA}$ variation reflects the relative oceanic moisture contribution related to the large-scale atmospheric circulation between the NIO and PO across different PDO phases (Fig. 6d, e). We find that such a decadal signal is recorded in the published stalagmite $\delta^{18}O$ in Shihua Cave[55] (Fig. 5d). Our CAM3 tagging simulation data shed light on

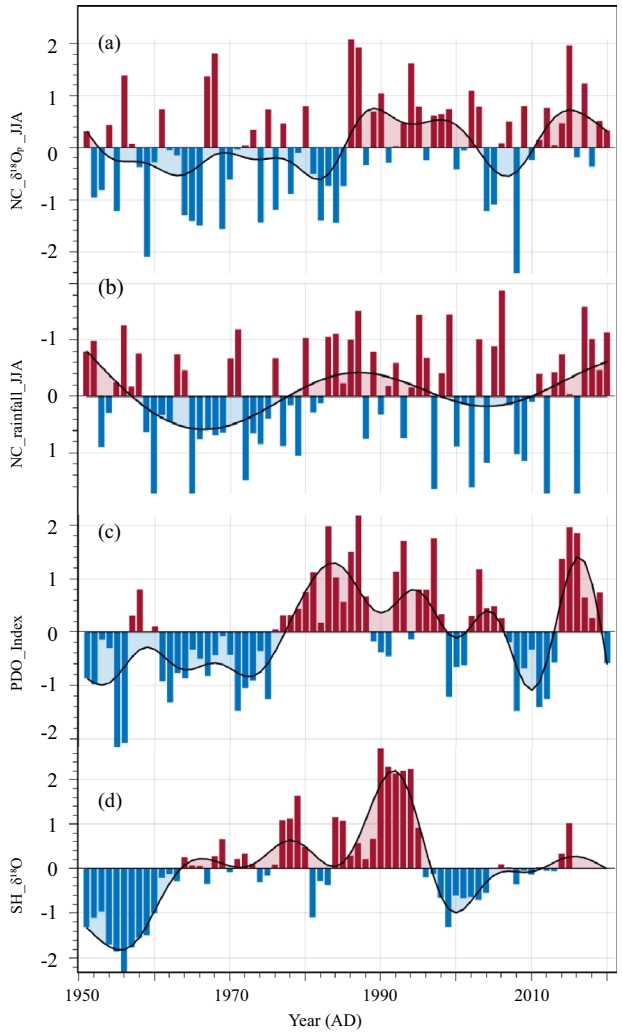

Fig. 5 Time-series comparisons. *Z* score transformed time-series comparisons between **a** the modeled JJA amount weighted precipitation $\delta^{18}O$ in northern China, **b** the modeled JJA precipitation in northern China, **c** the Pacific Decadal Oscillation index, **d** stalagmite $\delta^{18}O$ in Shihua Cave for 1951–2020. The black curves indicate the 7-year low-pass Butterworth filter.

potential mechanisms driving the decadal variability of the natural $\delta^{18}O$ record from this area.

DISCUSSION

Over the past two decades, stalagmite records have provided valuable insights into hydroclimate changes in the EASM region. However, the focus of stalagmite-based studies has mainly been on the monsoon region of southern China, with limited records from northern China, particularly modern ones, hindering accurate interpretations of stable isotopic records in this region. In this context, our analysis contributes to a better understanding of the role of various moisture sources on $\delta^{18}O_p$ in northern China on the seasonal to decadal time scale.

Our data highlight the significantly distinct controlling factors for northern China $\delta^{18}O_p$ composition in different seasons. During the non-monsoon season, the $\delta^{18}O_p$ is primarily influenced by the temperature effect, resulting in the lowest and highest values in the winter and the pre-monsoon seasons, respectively. During the monsoon season, there is actually a large shift in moisture sources, contributions from the LLA, PO, and NIO (17.8%, 24.4%, and 13.0%, respectively) are significant moisture sources impacting the summer $\delta^{18}O_p$. Our results suggest that summer $\delta^{18}O_p$ and $\delta^{18}O_s$ variability in northern China reflect large-scale changes in moisture source and dynamic interplay of upstream convection processes.

Moreover, this study provides further evidence that the variation of oceanic moisture from the PO and the NIO plays a vital role in the decadal variation of the $\delta^{18}O_{p\_JJA}$, which is modulated by the atmospheric circulation anomalies influenced by PDO. While our study emphasizes the dominant role of moisture sources in influencing the decadal variation of $\delta^{18}O_{p\_JJA}$, we acknowledge that $\delta^{18}O_{p\_JJA}$ in northern China also serves as an indicator of long-term precipitation changes. These changes can arise not just from the "amount effect", but also from shifts in the relative contributions of different moisture sources. Taken together, the interpretation of decadal $\delta^{18}O_{p\_JJA}$ and $\delta^{18}O_s$ variation in northern China can be potentially interpreted in a framework of overall changes in the moisture source dynamics and regional precipitation intensity.

METHODS

CAM3 model design and applications

The CAM3 was developed at the National Center for Atmospheric Research (NCAR) with a horizontal resolution of 2.8° × 2.8°, and 26 verticals with the model top at 3.5 hPa[29]. We chose the finite-volume core (CAM-FV) to ensure optimal mass and energy balance, separating the dynamical core from physical parameterization through a time-split approximation[29,56,57]. CAM3 employs the Community Land Model as its surface scheme[58] and uses a prognostic parameterization for its cloud water scheme, initially developed by Rasch and Kristjánsson[59] and later updated by Zhang et al.[60]. Convective cloud fraction is calculated using functions of convective updraft mass flux, following the approach of Xu and Krueger[61].

A moisture-tagging module is integrated into CAM3[62], providing the amount of water vapor from each source region that turns into precipitation at each grid for each month[63,64]. This module employs additional tracers for each source region to tag and track the water vapor from evaporation to precipitation[62,65,66]. Additionally, CAM3 has a stable water isotopes module, which allows the simulation of isotopic fractionation processes related to surface evaporation and cloud physics[29,67,68].

Statistical methods for correlation analysis

We employed the least-squares linear regression method to calculate the linear Pearson correlation coefficients between the independent and dependent variables. To establish the confidence intervals for these coefficients, we employed a pairwise moving-block bootstrap method using the PearsonT3 software[69]. The block length of this bootstrap method was determined on average proportional to the estimated data autocorrelation. This approach effectively preserves the serial dependence of time-series data and provides corrected 95% confidence intervals that remain valid in the presence of autocorrelation. The coverage accuracy is increased by applying calibration to standard error-based bootstrap Student's t confidence interval.

In the statistical significance of field correlations (i.e., Fig. 4), we implemented the false discovery rate (FDR) procedure using a MATLAB code to control the proportion ($q = 5\%$) of falsely rejected null hypotheses, where q guarantees that 5% or fewer of the locations where the null hypothesis is rejected are false detections[70]. FDR generally provides a more robust method for

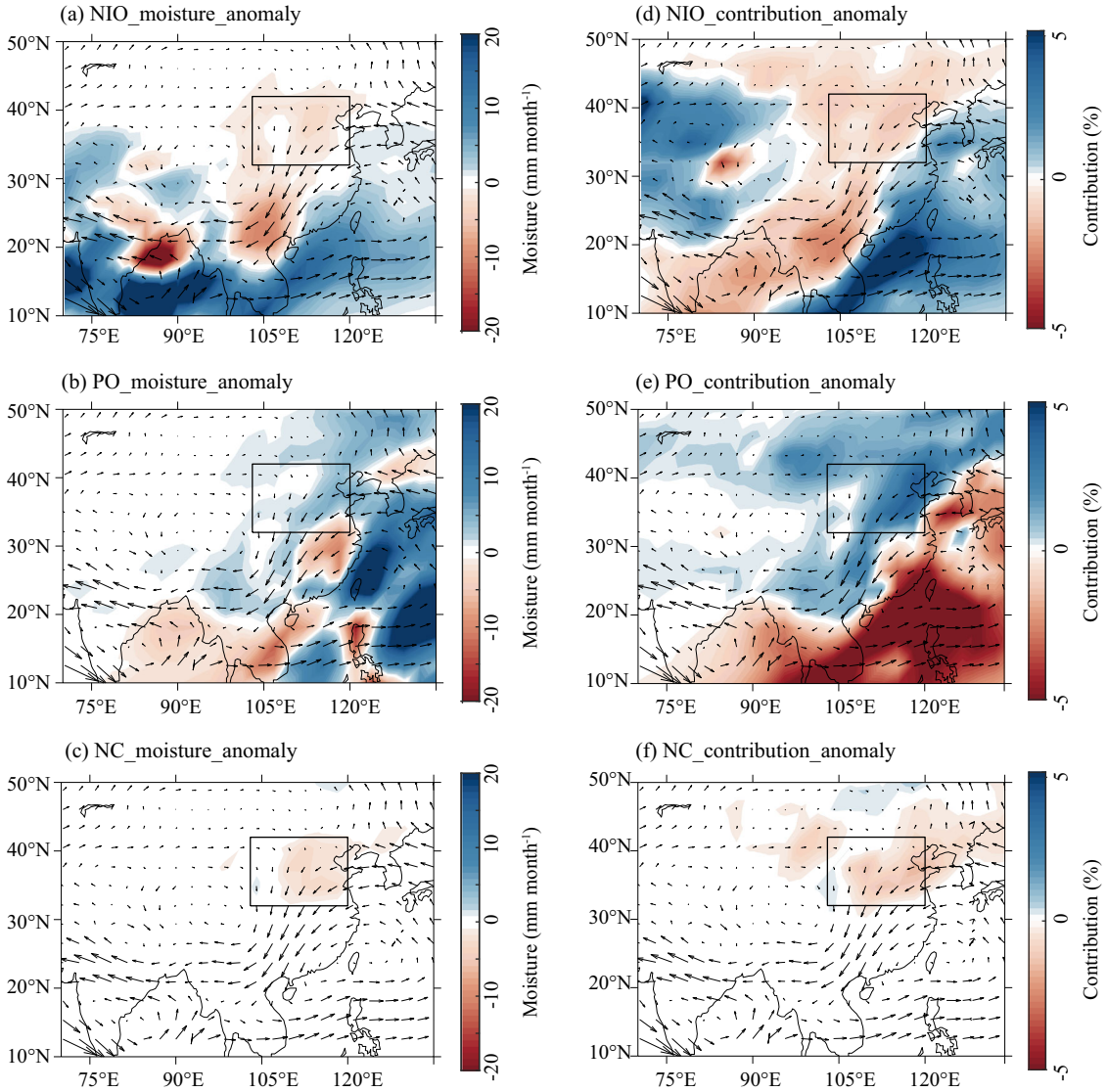

Fig. 6 Positive minus negative PDO phase JJA tagged moisture and contribution anomalies. a–c JJA moisture anomalies from NIO (**a**), PO (**b**), and NC (**c**) are superimposed by simulated vertically integrated moisture flux anomalies. **d–f** JJA moisture contribution anomalies from NIO (**d**), PO (**e**), and NC (**f**) are superimposed by simulated vertically integrated moisture flux anomalies. The black box represents the defined areas for northern China.

correcting for multiple comparisons[71,72] than procedures like Bonferroni correction that provide robust control of the familywise error rate (i.e., the probability that one or more null hypotheses are mistakenly rejected).

DATA AVAILABILITY

The CAM3 modeling data is available in the East Asian Paleoenvironmental Science Database (https://doi.org/10.12262/IEECAS.EAPSD2023014). Other data used in this study is publicly available: The CAM3 simulation model is available at http://www.cesm.ucar.edu/models/atm-cam/download/. The CRU TS4.10 data from the Climate Research Unit is available at https://crudata.uea.ac.uk/cru/data/hrg/. The GPCP 2.3 data from the Global Precipitation Climatology Project is available at https://psl.noaa.gov/data/gridded/data.gpcp.html. Sea surface temperature data can be obtained from https://www.metoffice.gov.uk/hadobs/hadisst/. The Global Network of Isotopes in Precipitation (GNIP) data is provided by the International Atomic Energy Agency (https://nucleus.iaea.org/wiser).

CODE AVAILABILITY

The MATLAB code for estimating the FDR[70] is available at https://www.mathworks.com/matlabcentral/fileexchange/71734-fdr. Any requests for code or data can be directed to the authors.

Received: 3 August 2023; Accepted: 1 January 2024;
Published online: 10 January 2024

REFERENCES

1. Caley, T., Roche, D. M. & Renssen, H. Orbital Asian summer monsoon dynamics revealed using an isotope-enabled global climate model. *Nat. Commun.* **5**, 1–6 (2014).
2. Cheng, H. et al. The Asian monsoon over the past 640,000 years and ice age terminations. *Nature* **534**, 640–646 (2016).
3. Chiang, J. C., Herman, M. J., Yoshimura, K. & Fung, I. Y. Enriched East Asian oxygen isotope of precipitation indicates reduced summer seasonality in regional climate and westerlies. *Proc. Natl Acad. Sci. USA* **117**, 14745–14750 (2020).

4. Pausata, F. S. R., Battisti, D. S., Nisancioglu, K. H. & Bitz, C. M. Chinese stalagmite d^{18}O controlled by changes in the Indian monsoon during a simulated Heinrich event. *Nat. Geosci.* **4**, 474–480 (2011).
5. Wang, Y. J. et al. A high-resolution absolute-dated late Pleistocene Monsoon record from Hulu Cave, China. *Science* **294**, 2345–2348 (2001).
6. Cheng, H. et al. Orbital-scale Asian summer monsoon variations: paradox and exploration. *Sci. China-Earth Sci.* **64**, 529–544 (2021).
7. Zhang, H. W. et al. A data-model comparison pinpoints Holocene spatiotemporal pattern of East Asian summer monsoon. *Quat. Sci. Rev.* **261**, 106911 (2021).
8. Cai, Z. Y. & Tian, L. D. Atmospheric controls on seasonal and interannual variations in the precipitation isotope in the East Asian Monsoon region. *J. Clim.* **29**, 1339–1352 (2016).
9. Cai, Z. Y., Tian, L. D. & Bowen, G. J. Spatial-seasonal patterns reveal large-scale atmospheric controls on Asian Monsoon precipitation water isotope ratios. *Earth Planet. Sci. Lett.* **503**, 158–169 (2018).
10. Ruan, J. Y., Zhang, H. Y., Cai, Z. Y., Yang, X. Q. & Yin, J. Regional controls on daily to interannual variations of precipitation isotope ratios in Southeast China: implications for paleomonsoon reconstruction. *Earth Planet. Sci. Lett.* **527**, 115794 (2019).
11. Yang, H., Johnson, K. R., Griffiths, M. & Yoshimura, K. Interannual controls on oxygen isotope variability in Asian monsoon precipitation and implications for paleoclimate reconstructions. *J. Geophys. Res* **121**, 8410–8428 (2016).
12. Baker, A. J. et al. Seasonality of westerly moisture transport in the East Asian Summer Monsoon and its implications for interpreting precipitation δ^{18}O. *J. Geophys. Res. Atmos.* **120**, 5850–5862 (2015).
13. Tan, M. Circulation effect: response of precipitation δ^{18}O to the ENSO cycle in monsoon regions of China. *Clim. Dyn.* **42**, 1067–1077 (2014).
14. Tan, L. C. et al. Climate significance of speleothem δ^{18}O from central China on decadal timescale. *J. Asian Earth Sci.* **106**, 150–155 (2015).
15. Lin, F. Y. et al. Seasonality of precipitation recorded in a modern (1907–2008) annually laminated stalagmite from central China. *Palaeogeogr. Palaeoclimatol. Palaeoecol.* **576**, 110489 (2021).
16. Zhang, H. W. et al. A 200-year annually laminated stalagmite record of precipitation seasonality in southeastern China and its linkages to ENSO and PDO. *Sci. Rep.* **8**, 12344 (2018).
17. Zhang, H. W. et al. Effect of precipitation seasonality on annual oxygen isotopic composition in the area of spring persistent rain in southeastern China and its paleoclimatic implication. *Clim. Past* **16**, 211–225 (2020).
18. Zhang, J. Y. et al. Coupled effects of moisture transport pathway and convection on stable isotopes in precipitation in East Asia: implications for paleoclimate reconstruction. *J. Clim.* **34**, 9811–9822 (2021).
19. Araguás, L., Froehlich, K. & Rozanski, K. Stable isotope composition of precipitation over Southeast Asia. *J. Geophys. Res. Atmos.* **103**, 28721–28742 (1998).
20. Liu, J., Song, X., Yuan, G., Sun, X. & Yang, L. Stable isotopic compositions of precipitation in China. *Tellus B* **66**, 22567 (2014).
21. Hua, L., Zhong, L. & Ke, Z. Characteristics of the precipitation recycling ratio and its relationship with regional precipitation in China. *Theor. Appl. Climatol.* **127**, 513–531 (2015).
22. Li, X. F. et al. Recycled moisture in an enclosed basin, Guanzhong Basin of Northern China, in the summer: contribution to precipitation based on a stable isotope approach. *Environ. Sci. Pollut. Res.* **27**, 27926–27936 (2020).
23. Sun, C., Chen, W., Chen, Y. & Cai, Z. Stable isotopes of atmospheric precipitation and its environmental drivers in the eastern Chinese Loess Plateau, China. *J. Hydrol.* **581**, 124404 (2020).
24. Li, Y. et al. Variations of Stable Isotopic Composition in Atmospheric Water Vapor and their Controlling Factors – A 6-Year Continuous Sampling Study in Nanjing, Eastern China. *J. Geophys. Res. Atmos.* **125**, e2019JD031697 (2020).
25. Tang, Y. et al. Effects of changes in moisture source and the upstream rainout on stable isotopes in precipitation – a case study in Nanjing, eastern China. *Hydrol. Earth Syst. Sci.* **19**, 4293–4306 (2015).
26. Wang, D. et al. Vehicle-based in situ observations of the water vapor isotopic composition across China: spatial and seasonal distributions and controls. *Atmos. Chem. Phys.* **23**, 3409–3433 (2023).
27. Xie, C. et al. Precipitation stable isotope composition, moisture sources, and controlling factors in Xi'an, Northwest China. *Atmos. Res.* **280**, 106428 (2022).
28. Yu, W. et al. Stable oxygen isotope differences between the areas to the north and south of Qinling Mountains in China reveal different moisture sources. *Int. J. Climatol.* **34**, 1760–1772 (2014).
29. Collins, W. D. et al. The formulation and atmospheric simulation of the Community Atmosphere Model version 3 (CAM3). *J. Clim.* **19**, 2144–2161 (2006).
30. Hu, J., Emile-Geay, J., Tabor, C., Nusbaumer, J. & Partin, J. Deciphering oxygen isotope records from Chinese speleothems with an isotope-enabled climate model. *Paleoceanogr. Paleoclimatol.* **34**, 2098–2112 (2019).
31. Liu, X. D., Xie, X. X., Guo, Z. T., Yin, Z. Y. & Chen, G. S. Model-based orbital-scale precipitation δ^{18}O variations and distinct mechanisms in Asian monsoon and arid regions. *Natl. Sci. Rev.* **9**, 11 (2022).
32. Cai, Z. Y., Tian, L. D. & Bowen, G. J. ENSO variability reflected in precipitation oxygen isotopes across the Asian Summer Monsoon region. *Earth Planet. Sci. Lett.* **475**, 25–33 (2017).
33. Li, W. L., Wang, K. L., Fu, S. M. & Jiang, H. The interrelationship between regional westerly index and the water vapor budget in Northwest China. *J. Glaciol. Geocryol.* **30**, 28–34 (2008).
34. Li, J. X. et al. Narrow and wide India–Burma trough-like circulations: their different impacts on precipitation over southern China. *Geosci. Lett.* **9**, 7 (2022).
35. Yu, W. et al. Precipitation stable isotope records from the northern Hengduan Mountains in China capture signals of the winter India-Burma Trough and the Indian summer monsoon. *Earth Planet. Sci. Lett.* **477**, 123–133 (2017).
36. Ding, Y. & Chan, J. C. L. The East Asian summer monsoon: an overview. *Meteor. Atmos. Phys.* **89**, 117–142 (2005).
37. He, Y. et al. Impact of atmospheric convection on south Tibet summer precipitation isotopologue composition using a combination of in situ measurements, satellite data and atmospheric general circulation modeling. *J. Geophys. Res.* **120**, 3852–3871 (2015).
38. Maher, B. A. & Thompson, R. Oxygen isotopes from Chinese caves: records not of monsoon rainfall but of circulation regime. *J. Geophys. Res. Atmos.* **27**, 615–624 (2012).
39. Ishizaki, Y. Interannual variability of H^{18}_2O in precipitation over the Asian monsoon region. *J. Geophys. Res.* **117**, D16308 (2012).
40. Wang, D. et al. Indian monsoon precipitation isotopes linked with high level cloud cover at local and regional scales. *Earth Planet. Sci. Lett.* **529**, 115837 (2020).
41. Wang, B. & Xu, X. H. Northern Hemisphere summer monsoon singularities and climatological intraseasonal oscillation. *J. Clim.* **10**, 1171–1185 (1997).
42. Axelsson, J. et al. A precipitation isotopic response in 2014–2015 to moisture transport changes in the Central Himalayas. *J. Geophys. Res. Atmos.* **128**, e2023JD038568 (2023).
43. Bowen, G. J., Cai, Z. Y., Fiorella, R. P. & Putman, A. Isotopes in the water cycle: regional- to global-scale patterns and applications. *Annu. Rev. Earth Planet. Sci.* **47**, 453–479 (2019).
44. Galewsky, J. et al. Stable isotopes in atmospheric water vapor and applications to the hydrologic cycle. *Rev. Geophys.* **54**, 809–865 (2016).
45. Wang, Y. & Zhou, L. Observed trends in extreme precipitation events in China during 1961–2001 and the associated changes in large-scale circulation. *Geophys. Res. Lett.* **32**, L09707 (2005).
46. Han, J. & Wang, H. Interdecadal variability of the East Asian summer monsoon in an AGCM. *Adv. Atmos. Sci.* **24**, 808–818 (2007).
47. Jiang, Z. et al. Impact of moisture source variation on decadal-scale changes of precipitation in China from 1951 to 2010. *J. Geophys. Res. Atmos.* **122**, 600–613 (2017).
48. Piao, J., Chen, W., Chen, S., Gong, H. & Zhang, Q. Summer water vapor sources in Northeast Asia and East Siberia revealed by a moisture-tracing atmospheric model. *J. Clim.* **33**, 3883–3899 (2020).
49. Qian, C. & Zhou, T. Multidecadal variability of North China aridity and its relationship to PDO during 1900–2010. *J. Clim.* **27**, 1210–1222 (2014).
50. Xu, Z. Q., Fan, K. & Wang, H. J. Decadal variation of summer precipitation over China and associated atmospheric circulation after the late 1990s. *J. Clim.* **28**, 4086–4106 (2015).
51. Zhu, Y., Wang, H., Zhou, W. & Ma, J. Recent changes in the summer precipitation pattern in East China and the background circulation. *Clim. Dyn.* **36**, 1463–1473 (2011).
52. Piao, J. et al. An abrupt rainfall decrease over the Asian inland plateau region around 1999 and the possible underlying mechanism. *Adv. Atmos. Sci.* **34**, 456–468 (2017).
53. Huang, Y., Wang, H., Fan, K. & Gao, Y. The western Pacific subtropical high after the 1970s: Westward or eastward shift? *Clim. Dyn.* **44**, 2035–2047 (2015).
54. Krklec, K., Domínguez-Villar, D. & Lojen, S. The impact of moisture sources on the oxygen isotope composition of precipitation at a continental site in central Europe. *J. Hydrol.* **561**, 810–821 (2018).
55. Li, X. L. et al. The East Asian summer monsoon variability over the last 145 years inferred from the Shihua Cave record, North China. *Sci. Rep.* **7**, 7078 (2017).
56. Lin, S. J. "vertically Lagrangian" finite-volume dynamical core for global models. *Mon. Weather Rev.* **132**, 2293–2307 (2004).
57. Williamson, D. L. Time-split versus process-split coupling of parameterizations and dynamical core. *Mon. Weather Rev.* **130**, 2024–2041 (2002).
58. Dickinson, R. E. et al. The Community Land Model and its climate statistics as a component of the Community Climate System Model. *J. Clim.* **19**, 2302–2324 (2006).
59. Rasch, P. & Kristjánsson, J. A comparison of the CCM3 model climate using diagnosed and predicted condensate parameterizations. *J. Clim.* **11**, 1587–1614 (1998).

60. Zhang, M., Lin, W., Bretherton, C. S., Hack, J. J. & Rasch, P. J. A modified formulation of fractional stratiform condensation rate in the NCAR Community Atmospheric Model (CAM2). *J. Geophys. Res.* **108**, 4035 (2003).
61. Xu, K. M. & Krueger, S. K. Evaluation of cloudiness parameterizations using a cumulus ensemble model. *Mon. Weather Rev.* **119**, 342–367 (1991).
62. Koster, R., Jouzel, J., Suozzo, R. & Russell, G. Global sources of local precipitation as determined by the NASA/GISS GCM. *Geophys. Res. Lett.* **13**, 121–124 (1986).
63. Numaguti, A. Origin and recycling processes of precipitating water over the Eurasian continent: experiments using an atmospheric general circulation model. *J. Geophys. Res. Atmos.* **104**, 1957–1972 (1999).
64. Trenberth, K. E. Atmospheric moisture residence times and cycling: implications for rainfall rates with climate change. *Clim. Change* **39**, 667–694 (1998).
65. Delaygue, G., Masson, V., Jouzel, J., Koster, R. D. & Healy, R. J. The origin of Antarctic precipitation: a modelling approach. *Tellus B* **52**, 19–36 (2000).
66. Werner, M., Heimann, M. & Hoffmann, G. Isotopic composition and origin of polar precipitation in present and glacial climate simulations. *Tellus B* **53**, 53–71 (2001).
67. Noone, D. & Simmonds, I. Annular variations in moisture transport mechanisms and the abundance of $\delta^{18}O$ in Antarctic snow. *J. Geophys. Res.* **107**, 4742 (2002).
68. Salih, A. A. M., Zhang, Q., Pausata, F. S. R. & Tjernstrom, M. Sources of Sahelian-Sudan moisture: insights from a moisture-tracing atmospheric model. *J. Geophys. Res.* **121**, 7819–7832 (2016).
69. Ólafsdóttir, K. B. & Mudelsee, M. More accurate, calibrated bootstrap confidence intervals for estimating the correlation between two timeseries. *Math. Geosci.* **46**, 411–427 (2014).
70. Gerber, M. E. FDR (False Discovery Rate) (https://www.mathworks.com/matlabcentral/fileexchange/71734-fdrfalse-discovery-rate), MATLAB Central File Exchange. Retrieved February. **17** (2021).
71. Benjamini, Y. & Hochberg, Y. Controlling the false discovery rate: a practical and powerful approach to multiple testing. *J. R. Stat. Soc. Ser. B (Methodol.)* **57**, 289–300 (1995).
72. Ventura, V., Paciorek, C. J. & Risbey, J. S. Controlling the proportion of falsely rejected hypotheses when conducting multiple tests with climatological data. *J. Clim.* **17**, 4343–4356 (2004).

ACKNOWLEDGEMENTS

This work was supported by the National Natural Science Foundation (42325705), Chinese Academy of Sciences (xbzg-zdsys-202217, XDB40000000, 2020VCA0019), and the Swedish Research Council (Vetenskapsrådet, grant no. 2022-03129). The CAM3 simulation and data analysis were performed using resources provided by the Swedish National Infrastructure for Computing (SNIC) at the National Supercomputer Centre (NSC), which is partially funded by the Swedish Research Council through grant agreement no. 2022-06725 and no. 2018-05973.

AUTHOR CONTRIBUTIONS

F.L.: formal analysis, data curation, investigation, visualization, writing, and original draft. Q.Z.: investigation, resources, funding acquisition, supervision, and editing. A.S.: methodology, investigation, validation, review, and editing. Z.W.: data curation, software. J.A.: review and editing. L.C.: investigation, review & editing. T.W.: review & editing. L.T.: investigation, validation, project administration, funding acquisition, supervision, review & editing.

COMPETING INTERESTS

The authors declare no competing interests.

ADDITIONAL INFORMATION

Supplementary information The online version contains supplementary material available at https://doi.org/10.1038/s41612-024-00564-x.

Correspondence and requests for materials should be addressed to Qiong Zhang or Liangcheng Tan.